



Hydrothermal synthesized $\alpha\text{-Fe}_2\text{O}_3/\text{Mn}_2\text{O}_3$ nanocomposite for efficient photodegradation of methylene blue under visible light

Aliakbar Dehno Khalaji

Department of Chemistry, Faculty of Science, Golestan University, Gorgan, Iran

Received: 19 December 2024; Accepted: 4 May 2025

*Corresponding author, E-mail: alidkhalaji@yahoo.com

ABSTRACT

Treating wastewater using transition metal oxide nanocomposites as efficient photocatalysts has received more attention in recent years. In this work, to develop a new efficient photocatalyst based on metal oxides was developed by preparing the $\alpha\text{-Fe}_2\text{O}_3/\text{Mn}_2\text{O}_3$ heterojunction nanocomposite was prepared via a facile one-pot hydrothermal precipitation technique. The nanocomposite was characterized using FT-IR, XRD, UV-Vis, PL, SEM and TEM techniques. The results confirm the successful formation of $\alpha\text{-Fe}_2\text{O}_3/\text{Mn}_2\text{O}_3$ nanocomposite. The as-prepared $\alpha\text{-Fe}_2\text{O}_3/\text{Mn}_2\text{O}_3$ was assessed for the photodegradation of methylene blue (MB) as a model wastewater under visible light irradiation. The photocatalytic activity for degradation of MB was calculated to be 96.7% within 90 min. The kinetics of experimental data were studied using the Langmuir mechanism, resulting in a rate constant of 0.02521 min^{-1} . The effect of different scavengers on photodegradation efficiency was investigated and the results predicted that the $\text{O}_2^{\cdot -}$ radicals are responsible for the degradation of MB dye molecules. The reusability after six cycles was studied without significant activity change, confirming the photocatalytic efficiency and stability of $\alpha\text{-Fe}_2\text{O}_3/\text{Mn}_2\text{O}_3$ nanocomposite. Therefore, the as-prepared $\alpha\text{-Fe}_2\text{O}_3/\text{Mn}_2\text{O}_3$ is a promising photocatalyst in the photodegradation of other organic dyes.

Keywords: Heterojunction, $\alpha\text{-Fe}_2\text{O}_3/\text{Mn}_2\text{O}_3$ nanocomposite, Methylene blue, Photodegradation.

1. Introduction

Recently, heterojunction metal oxide semiconductors have great attention for their unique properties and novel potential applications in various fields due to their small size and high surface area [1-3]. Among the various transition metal oxide semiconductors, hematite ($\alpha\text{-Fe}_2\text{O}_3$), an n-type semiconductor with a low band gap of 2-2.3 eV, chemically stable, low-cost and non-toxic is the most metal oxide that could be utilized in the photodegradation of different organic dyes [4-6]. Today, water purification is an important challenge for human health across the world [7,8].

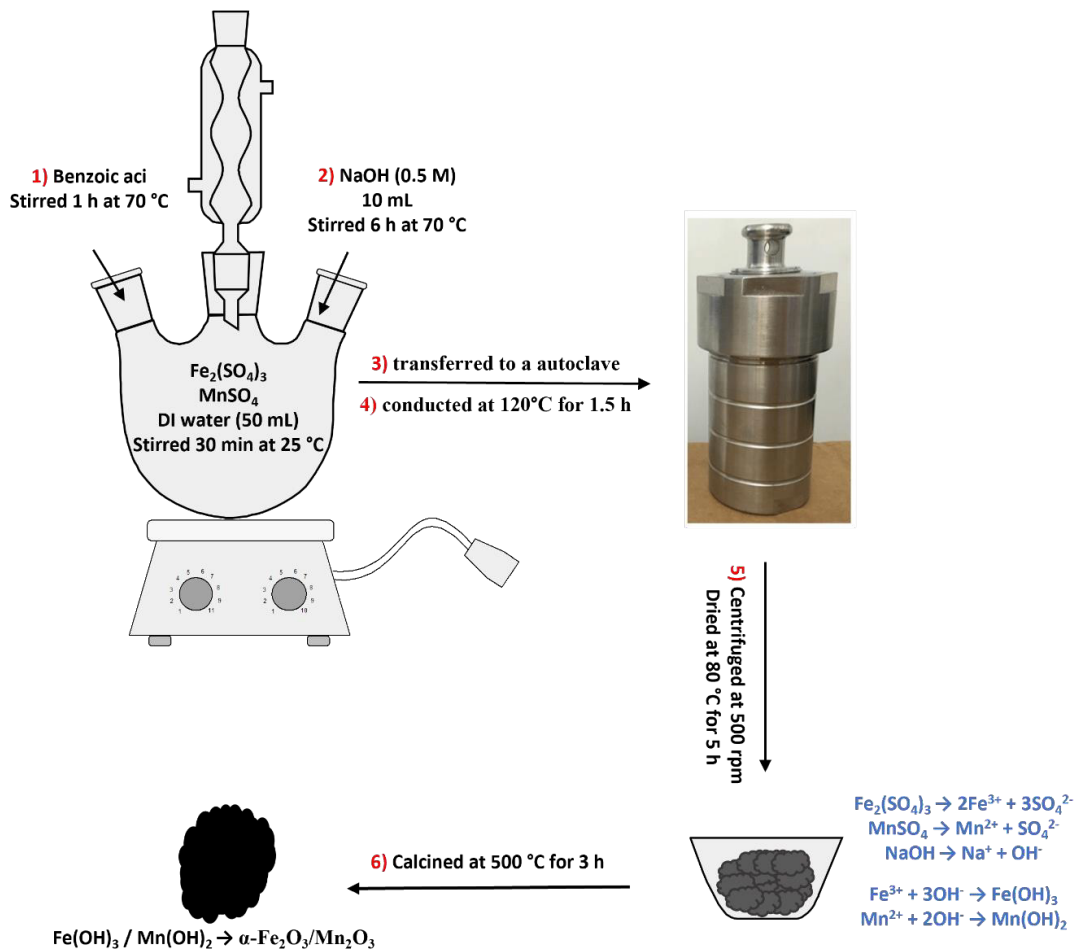
Due to various industrial activities, the production capacity of them is more than 700000 tons annually [9]. Therefore, many dangerous organic dyes, 140000 tons over 10000 types of dyes [9], were released into the environment, especially water resources, which can affect water gas solubility, transparency and lead to serious environmental imbalances [10]. Wastewater including organic dyes has a cancer-causing impact on human health [3] because organic dyes are very stable, toxic, and non-biodegradable [11-13]. Now, many techniques have been used to remove organic dyes from wastewater such as adsorption [14-16], coagulation

[17-20], and advanced oxidation [21-25]. The main disadvantage of these techniques is that they transfer the different organic dyes between two different phases, leading to a secondary pollutant. Therefore, the development of an efficient technique such as photocatalytic degradation has become a necessity [26-32]. Recently, nanocomposites prepared from two different metal oxides exhibit high catalytic properties under light irradiation to degrade different organic dyes [33-37]. For example, heterojunction $\alpha\text{-Fe}_2\text{O}_3\text{-ZnO}$ and $\alpha\text{-Fe}_2\text{O}_3\text{-Cu}_2\text{O}$ nanocomposites were synthesized and used for the degradation of methylene blue in an aqueous solution [4,5]. Two-dimensional $\text{CuO-Fe}_2\text{O}_3$ nanocomposites were prepared by a simple hydrothermal technique and used as a photocatalyst to degrade rhodamine B under simulated sunlight [38]. By the precipitation and modified sol-gel auto-combustion methods, $\text{Fe}_2\text{O}_3\text{-CeO}_2$ nanocomposites were synthesized and used for the degradation of congo red under visible light irradiation [6]. Rini et al. [33] successfully synthesized

CoO/ZnO nanocomposite for enhancing the photodegradation of methylene blue. 100% removal of reactive blue dye within 2 h was done by the as-prepared $\text{TiO}_2/\text{Fe}_2\text{O}_3$ nanocomposites [34]. $\text{Co}_3\text{O}_4/\text{NiO}$ was prepared via an environment-friendly technique for photodegradation of methylene blue (92.8%) within 80 min [35].

In recent years, many articles have been reported on the synthesis of $\alpha\text{-Fe}_2\text{O}_3/\text{Mn}_2\text{O}_3$ nanocomposite with different applications. For example, coral-like $\text{Mn}_2\text{O}_3/\text{Fe}_2\text{O}_3$ nanocomposite was synthesized by a one-step surfactant-mediated co-precipitation for removal of H_2S [39], dye degradation [40,41], as anode material for lithium-ion batteries [42], lead (II) removal from industrial wastewater [43] and the photocatalytic oxidation process in As(III) removal from contaminated water [44].

This work aims to synthesize a new heterojunction $\alpha\text{-Fe}_2\text{O}_3/\text{Mn}_2\text{O}_3$ nanocomposite (Scheme 1) via the hydrothermal precipitate technique and study its photodegradation efficiency towards methylene blue under visible light.



Scheme. 1- Synthesis schematic of $\alpha\text{-Fe}_2\text{O}_3/\text{Mn}_2\text{O}_3$.

2. Experimental

2.1. Materials

$\text{Fe}_2(\text{SO}_4)_3$, MnSO_4 , benzoic acid, NaOH were purchased from Merck company and used as received without further purification.

2.2. Characterization

FT-IR spectrum was recorded using a Perkin-Elmer spectrometer in the range of 400-4000 cm^{-1} . The crystalline phase was determined by a Shimadzu 6100 X-ray diffractometer with $\text{Cu-K}\alpha$ radiation and $\lambda = 1.5406 \text{ \AA}$ in the scan range of 20-70°. UV-Vis spectrum was performed by a Shimadzu UV-Vis 3600 PLUS analysis. The PL spectrum was recorded at room temperature by use of a Shimadzu RF-5301 PC spectrophotometer. The SEM images were carried out by a Thermo scientific Apreo S scanning electron microscope with an acceleration voltage of 200 kV.

2.3. Synthesis of $\alpha\text{-Fe}_2\text{O}_3/\text{Mn}_2\text{O}_3$

A 1:1 molar ratio of $\text{Fe}_2(\text{SO}_4)_3$ and MnSO_4 , was added to 50 mL deionized water and stirred for about 30 min at room temperature. Then, benzoic acid was added and the mixture was stirred at 70°C for 1 h followed by the addition of NaOH solution (10 mL, 0.5 M). The mixture was transferred to a 100 mL Teflon-lined stainless-steel autoclave, and conducted at 120°C for 1.5 h. After that, the gray precipitates of a mixture of $\text{Fe}(\text{OH})_3$ and $\text{Mn}(\text{OH})_2$ were collected by centrifuging, washed with deionized water, and dried at 80°C. Finally calcined at 500°C for 3h. The black powders $\alpha\text{-Fe}_2\text{O}_3/\text{Mn}_2\text{O}_3$ nanocomposite were washed with deionized water, dried at 80 °C and finally characterized by FT-IR, XRD, UV-Vis, PL, and SEM techniques.

2.4. Photocatalytic studies

Photodegradation of MB dye with a concentration of 30 mg/L catalyzed by as-prepared $\alpha\text{-Fe}_2\text{O}_3/\text{Mn}_2\text{O}_3$ nanocomposite was carried out by adding a suitable amount (0.005 g, 0.01 g, and 0.02 g) of catalyst to a 50 mL solution of MB dye. Initially, the mixture was stirred under the dark condition for 30 min. Then, the solution was irradiated under visible light to expose the MB dye molecules. Finally, 5 mL of the mixture was collected, and centrifuged and dye concentration was determined by UV-Vis spectrum. The photodegradation percentage was calculated by the following equation (eq. 1), where C_0 (mg/L) and C_t (mg/L) are the concentration of dyes at equilibrium and t time, respectively.

$$D (\%) = \{(C_0 - C_t) / C_0\} \times 100 \quad (1)$$

2.5. Reusability

After each photodegradation process, the $\text{Fe}_2\text{O}_3/$

Mn_2O_3 nanocomposite was centrifuged, washed with DI water and dried at 80 °C for 3 h. Then, it was poured to the HCl solution (20 mL, 0.1 M) and stirred for about 0.5 h. After that, the $\text{Fe}_2\text{O}_3/$ Mn_2O_3 nanocomposite was centrifuged, washed with NaOH solution (0.1 M) and DI water (20 mL), dried at 80 °C for 3 h and the dried product was used in a photodegradation process.

3. Results and discussion

3.1. Characterization

3.1.1. FT-IR Spectra

The FTIR provides important insights into the functional groups present in the synthesized sample. In the FT-IR spectrum of $\text{Fe}_2\text{O}_3/\text{Mn}_2\text{O}_3$ nanocomposite before the photodegradation process (Fig. 1a and 1b), the weak and broad bands observed at about 3380 cm^{-1} and 1645 cm^{-1} are assigned to the O-H vibration of water molecules adsorbed on the surface of as-prepared $\alpha\text{-Fe}_2\text{O}_3/$ Mn_2O_3 nanocomposite [4,5,45,46]. The sharp bands observed at 485 cm^{-1} , 533 cm^{-1} , 575 cm^{-1} , 605 cm^{-1} , and 670 cm^{-1} are assigned to the M-O and M-O-M vibration of as-prepared $\text{Fe}_2\text{O}_3/\text{Mn}_2\text{O}_3$ nanocomposite [8,14,45]. Similar vibration peaks were seen in the FT-IR spectrum of $\text{Fe}_2\text{O}_3/\text{Mn}_2\text{O}_3$ nanocomposite after the photodegradation process (Fig. 1c and 1d), confirming that the stability of the $\text{Fe}_2\text{O}_3/\text{Mn}_2\text{O}_3$ product after the photodegradation process.

3.1.2. XRD patterns

X-ray diffraction (XRD) is a versatile technique for the analysis of the phase composition and crystal structure of samples. Similar XRD patterns of $\text{Fe}_2\text{O}_3/\text{Mn}_2\text{O}_3$ nanocomposite before and after the photodegradation process were shown in Fig. 2a and 2b, respectively, confirming that the stability of the $\text{Fe}_2\text{O}_3/\text{Mn}_2\text{O}_3$ product after the photodegradation process. In the XRD pattern (Fig. 2), the diffraction peaks assigned to the $\alpha\text{-Fe}_2\text{O}_3$ were observed at 2θ values of 24.15 (012), 32.83 (104), 35.59 (110), 40.76 (006), 49.31 (024), 54.06 (116), 57.59 (122), 62.44 (214) and 64.01° (300) were matched with tetragonal structure of $\alpha\text{-Fe}_2\text{O}_3$ [45,46]. While, the diffraction peaks at 2θ values of 22.93 (211), 32.91 (222), 38.11 (400), 45.21 (332), 49.29 (431), 55.06 (440), 59.66 (611), 65.66 (662), 67.31 (631) and 69.06° (444) were matched with the tetragonal structure of Mn_2O_3 [47,48]. Using the Scherrer equation ($D = 0.9 \lambda / \beta \cos\theta$), the crystallite size was calculated at about 29.51 nm. The intensities of diffraction peaks confirm the good crystallinity of $\alpha\text{-Fe}_2\text{O}_3/\text{Mn}_2\text{O}_3$ nanocomposite. Also, the XRD pattern is free of impurities.

3.1.3. UV-Vis and PL spectra

The UV-Vis and PL spectra are shown in Figs.

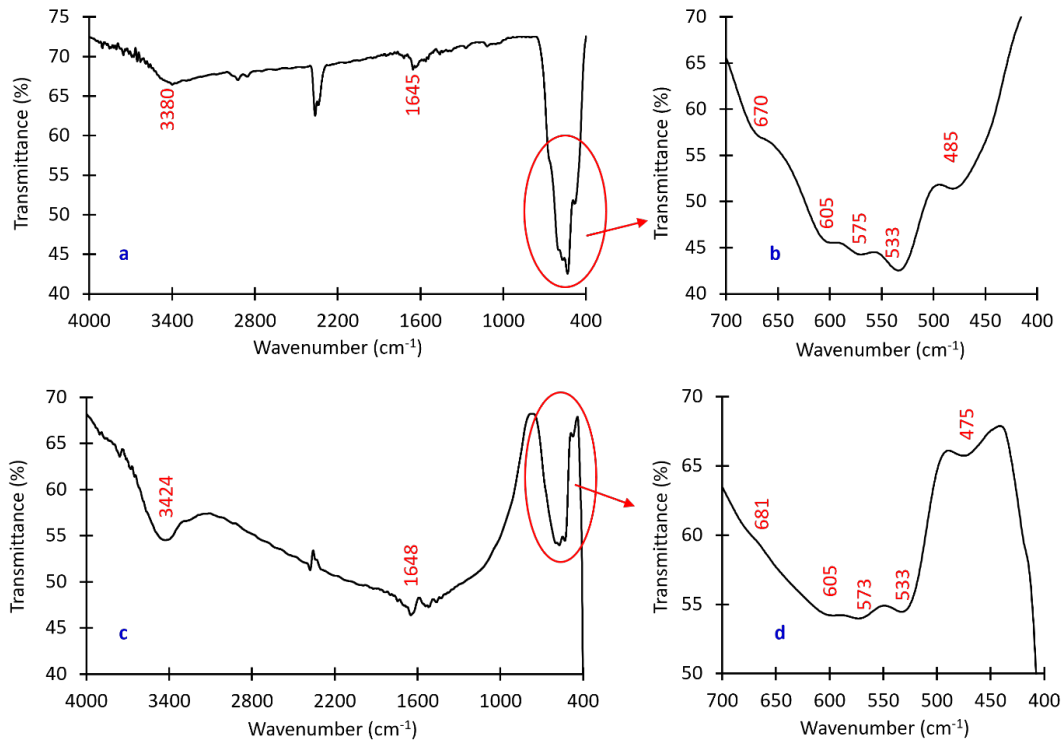


Fig. 1- FT-IR spectrum of as-prepared α -Fe₂O₃/Mn₂O₃ nanocomposite before (a,b) and after (c,d) MB photodegradation process.

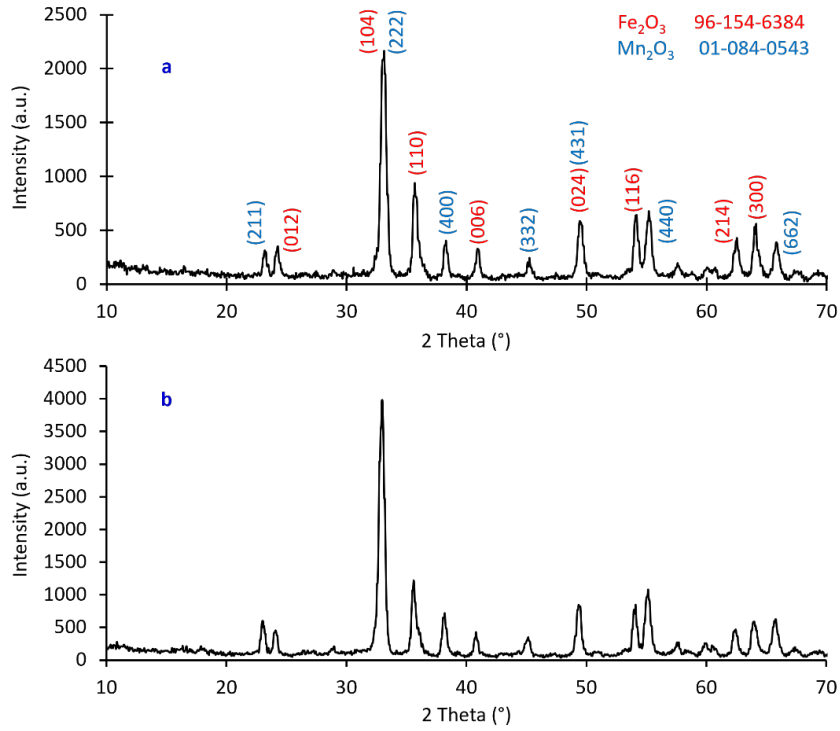


Fig. 2- XRD pattern of as-prepared α -Fe₂O₃/Mn₂O₃ nanocomposite a) before and b) after photodegradation process.

3a and 3b, respectively. It can be seen that the as-prepared $\alpha\text{-Fe}_2\text{O}_3/\text{Mn}_2\text{O}_3$ nanocomposite can be adsorbed light at about 210 nm assigned to the direct transition of electrons and 275 nm assigned to the surface plasmon resonance (SPR) (Fig. 3a) [49,50]. Also, a weak absorption peak is observed at about 575 nm assigned to the charge transfer [46].

In the PL spectrum (Fig. 3b), a strong luminescence band at 323 nm and two broad peaks at about 427 and 642 nm were observed, these are assigned to deep-level defects and the recombination of electrons and holes at oxygen vacancies of the $\text{Fe}_2\text{O}_3/\text{Mn}_2\text{O}_3$ nanocomposite [51-53].

3.1.4. SEM and TEM images

Fe-SEM and TEM images of as-prepared $\alpha\text{-Fe}_2\text{O}_3/\text{Mn}_2\text{O}_3$ nanocomposite before and after the photodegradation process are shown in Fig. 4a-4d. The sample exhibits different shapes with high agglomerated together to form an irregular morphology. TEM results confirmed that the particle sizes are below 100 nm.

3.2. MB photodegradation

3.2.1. The effect of pH solution

The as-prepared $\alpha\text{-Fe}_2\text{O}_3/\text{Mn}_2\text{O}_3$ nanocomposite was used as a photocatalyst for the photodegradation

of methylene blue dye, which is generally present in different industrial wastewaters [54-58]. The results of photodegradation of MB under visible light at different pH solutions (2-12) (Fig. 5) demonstrated a high percentage degradation of 96.7% at pH of 10, 0.02 g catalyst, and 120 min irradiation time, due to the increased electrostatic force of attraction between the cationic MB molecules onto the negative charge surface of $\alpha\text{-Fe}_2\text{O}_3/\text{Mn}_2\text{O}_3$ nanocomposite. While, in a low pH solution, MB removal is low due to the competitive interactions between H^+ and MB molecules as a cationic dye, as well as, the repulsive force interactions between the surface protonated catalyst and MB molecules [11]. Therefore, suitable contact happened between dye molecules and photogenerated radical species ($\text{O}_2^{\cdot-}$ and OH^\bullet) [59-68].

3.2.2. The effect of irradiation time and catalyst dose

The effect of irradiation time and dose of catalyst on the photodegradation efficiency of MB were studied and the results were represented in Fig. 6. It can be seen that the degradation was increased with increases of catalyst dose and also irradiation time. Maximum degradation (96.7%) was observed for 120 min irradiation time and 0.02 g catalyst dose.

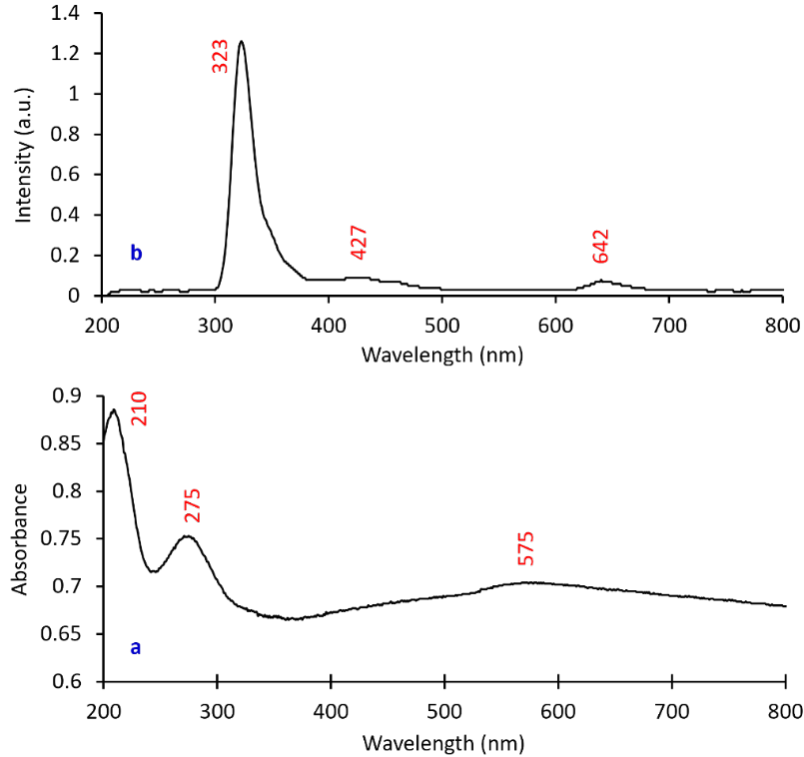


Fig. 3- a) UV-Vis and b) PL spectra of as-prepared $\alpha\text{-Fe}_2\text{O}_3/\text{Mn}_2\text{O}_3$ nanocomposite.

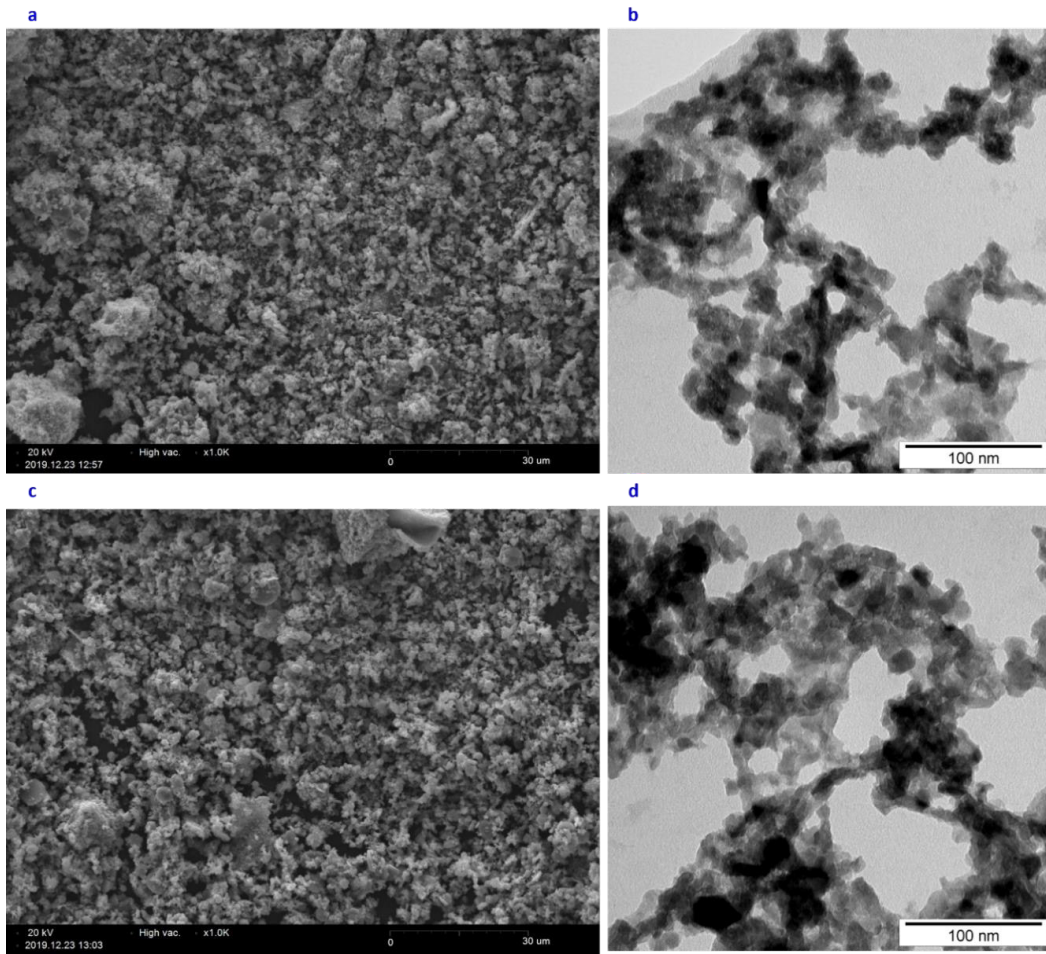


Fig. 4- SEM and TEM images of as-prepared $\alpha\text{-Fe}_2\text{O}_3/\text{Mn}_2\text{O}_3$ nanocomposite before (a,b) and after (c,d) photodegradation process.

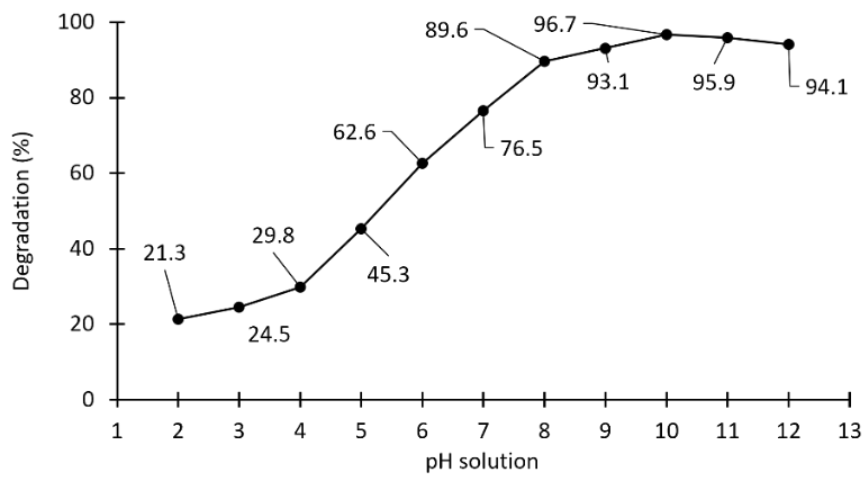


Fig. 5- The effect of initial pH solution on the photodegradation efficiency of MB.

The degradation of MB did not show an increase after 120 min, due to the exhausting of the surface sites [65]. Because of the increases in dose and time cause the increases of active sites and dye adsorbed on the surface of the catalyst, respectively [1,2,56]. Also, by increasing of dose catalyst from 0.005 to 0.02 g, the absorption of more light photons increases the number of electron-hole pairs producing more active radicals and finally, the MB photodegradation increases from 52.1% to 96.7% which is the future of heterogeneous catalysis [57-68].

3.2.3. Kinetic study

The Langmuir-Hinshelwood first-order reaction kinetics model (eq. 2) was used for studying the kinetics of MB dye removal under visible light irradiation using as-prepared $\alpha\text{-Fe}_2\text{O}_3/\text{Mn}_2\text{O}_3$ nanocomposite as a

catalyst. The results are shown in Fig. 7 and predicted that the process obeyed from pseudo-first-order with $R^2 = 0.9809$, confirming occurs the numerous processes during the photodegradation of MB [63]. The rate constant $k = 0.02521 \text{ min}^{-1}$ was calculated from the slope of the plot, while the $t_{1/2}$ (half-life time) value of 27.49 min was obtained using eq. 3 [4,5,26,28].

$$-\ln(C/C_0) = kt \tag{2}$$

$$t_{1/2} = 0.693 / k \tag{3}$$

3.2.4. Reusability

After the MB photodegradation process, the catalyst was collected, washed with HCl (0.1 M), and finally dried at 80°C for 3 h for each run. The

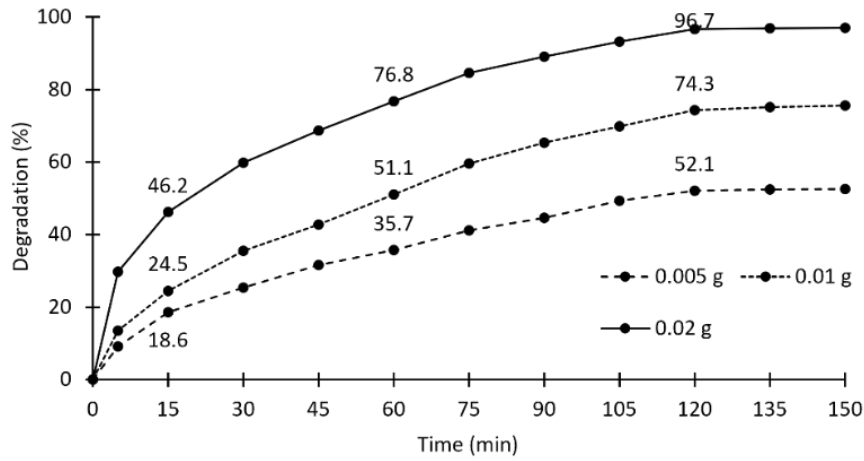


Fig. 6- The effect of irradiation time and catalyst dose on the photodegradation efficiency of MB.

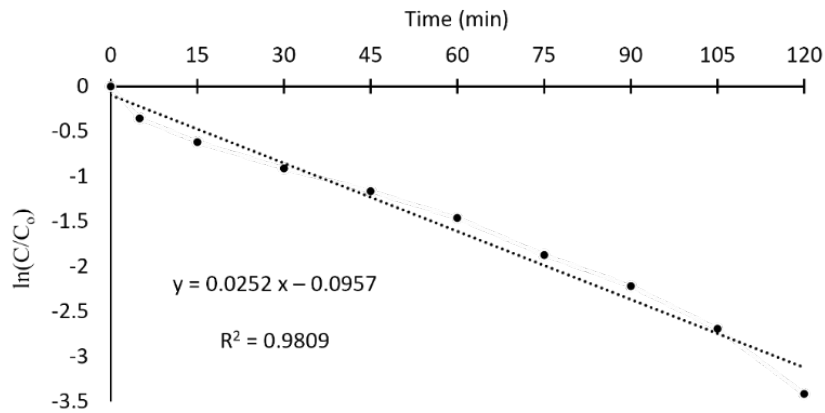


Fig. 7- $\ln(C/C_0)$ vs. time graph for the MB photodegradation efficiency.

photodegradation efficiency results for six runs are shown in Fig. 8. The degradation changed from 96.7% (initially) to 92.6% (sixth run), suggesting that the $\alpha\text{-Fe}_2\text{O}_3/\text{Mn}_2\text{O}_3$ nanocomposite was recyclable [11,33,36,63]. The decreases of MB photodegradation after 5 cycles can be attributed by 1) mass reduction throughout washing and drying and 2) the blocking pores and active site [33,36].

3.3. Photocatalytic mechanism

After visible light irradiation, the as-prepared

$\alpha\text{-Fe}_2\text{O}_3/\text{Mn}_2\text{O}_3$ nanocomposite produces an electron-hole pair. Then, the photoinduced holes and electrons can be reacted by O_2 and H_2O molecules to produce active superoxide and hydroxyl radicals ($\text{O}_2^{\cdot-}$ and OH^\bullet). Finally, these active radicals can be reacted with MB dye molecules adsorbed on the surface of the catalyst to degrade them to CO_2 and H_2O molecules and undergo a significant oxidation and reduction reactions [58-68]. The proposed MB dye photodegradation mechanism with details is shown in Scheme 2.

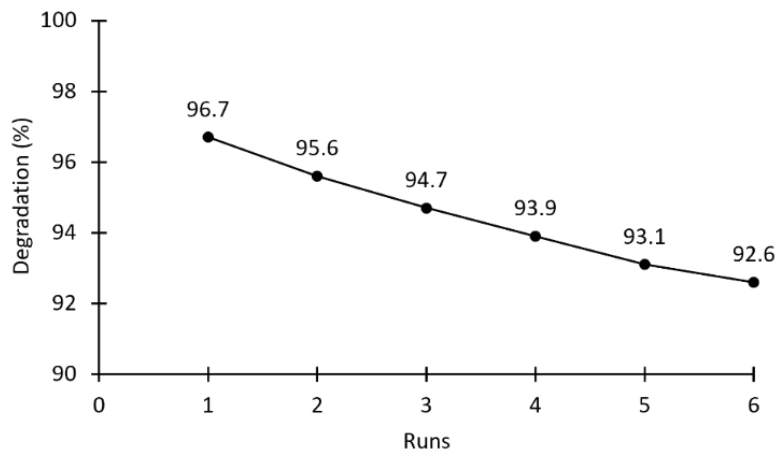
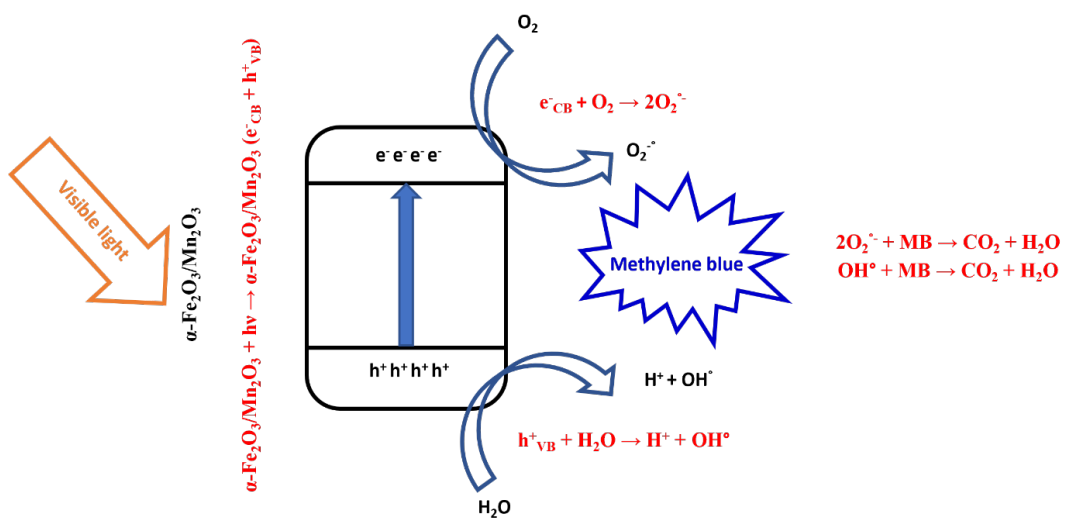


Fig. 8- Reusing of $\alpha\text{-Fe}_2\text{O}_3/\text{Mn}_2\text{O}_3$ nanocomposite for the MB photodegradation efficiency.



Scheme. 2- Schematic of MB photodegradation mechanism using $\alpha\text{-Fe}_2\text{O}_3/\text{Mn}_2\text{O}_3$ nanocomposite.

3.4. Trapping studies

The effect of various scavengers such as isopropanol (IP) [69], ethylenediaminetetraacetic acid (EDTA) [70] and benzoquinone (BQ) [71,72] in the MB photodegradation using $\alpha\text{-Fe}_2\text{O}_3/\text{Mn}_2\text{O}_3$ nanocomposite were utilized to scavenge active radicals such as OH° , h^+ , and O_2° , respectively, and the results are shown in Fig. 9. In the absence of any scavenger, the $\alpha\text{-Fe}_2\text{O}_3/\text{Mn}_2\text{O}_3$ nanocomposite had a 96.7% photodegradation efficiency towards MB dye. While, in the presence of IP, EDTA, and BQ the photodegradation efficiency was lowered to 84.6%, 59.8%, and 42.1%, respectively. These results confirmed that the O_2° radicals played a significant

role in the degradation of MB dye molecules rather than OH° radicals and h^+ [58,63,65,66].

3.5. Comparing with other MB catalysts

The maximum photodegradation efficiency of MB using an as-prepared $\alpha\text{-Fe}_2\text{O}_3/\text{Mn}_2\text{O}_3$ nanocomposite was compared with those of different other catalysts [33,35,36,58-68], and the results are shown in Table 1. The results predicted that the as-prepared has good photodegradation efficiency compared to other catalysts, suggesting that the $\alpha\text{-Fe}_2\text{O}_3/\text{Mn}_2\text{O}_3$ nanocomposite can be used as a suitable catalyst in wastewater treatment.

Table 1- Comparison of the photodegradation efficiency of MB with different catalysts

Catalysts	R (%)	Reference
ZnO	95.5	36
$\text{Co}_3\text{O}_4/\text{NiO}$	92.8	35
CoO/ZnO	67.5	33
Cu-MnO_2	100	58
BaO	85	59
Cd/ZnO	97	60
$\text{ZnO}/\text{N-CQD}$	80	61
$\text{NiFe}_2\text{O}_4/\text{CeO}_2$	82	62
$\text{Ag-CuFe}_2\text{O}_4$	99	63
$\text{SnO}_2\text{-CuO}$	90.3	64
$\text{g-C}_3\text{N}_4/\text{CoFe}_2\text{O}_4$	97.4	65
$\text{Co-ZnO}/\text{Fe}_3\text{O}_4$	88.72	66
Co/ZnO	97.5	67
$\alpha\text{-Fe}_2\text{O}_3$	78	68
$\alpha\text{-Fe}_2\text{O}_3/\text{Mn}_2\text{O}_3$	96.7	This work

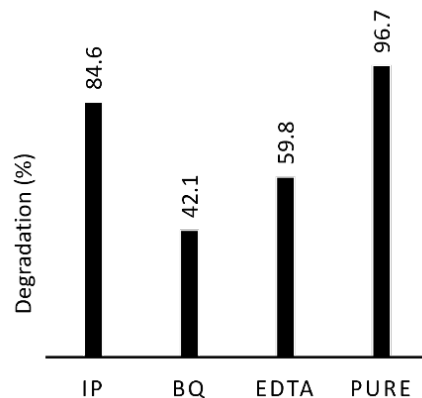


Fig. 9- The effect of scavengers in the photodegradation efficiency of $\alpha\text{-Fe}_2\text{O}_3/\text{Mn}_2\text{O}_3$ nanocomposite.

4. Conclusion

In summary, the heterojunction $\text{Fe}_2\text{O}_3/\text{Mn}_2\text{O}_3$ was prepared using a hydrothermal method and its photocatalytic activity for degrading methylene blue dye under visible light was investigated. Results showed that the important parameters such as pH, irradiation time, and catalyst dose significantly impact the degradation process. The degradation rate is very fast up to 30 min (59.8%) due to the unoccupied active sites on the surface of the photocatalyst and was achieved at 96.7% after 120 min at a pH value of 10. The degradation obeyed from the Langmuir-Hinshelwood first-order model with an R^2 value of 0.9809 with a rate constant of 0.02521 min^{-1} and $t_{1/2} = 27.49 \text{ min}$. The photodegradation efficiency of the catalyst changed from 96.7% to 92.6% after six recycles, predicting the stability of the catalyst. Trapping studies predicted that the $\text{O}_2^{\cdot -}$ radicals are responsible for the degradation of MB dye molecules. The results of this work predicted that the as-prepared $\alpha\text{-Fe}_2\text{O}_3/\text{Mn}_2\text{O}_3$ nanocomposite based photocatalyst is a simple and highly efficient route to decompose MB dye.

Acknowledgments

The author appreciates the support of this work by Golestan University.

References

- Panchal, P., Paul, D. R., Sharma, A., Hooda, D., Yadav, R., Meena, P., & Nehra, S. P. (2019). Phytoextract mediated ZnO/MgO nanocomposites for photocatalytic and antibacterial activities. *Journal of Photochemistry and Photobiology A: Chemistry*, 385, 112049.
- Haruna, M., Eshun, F., Bandoh, C. K., Agorku, E. S., Francis, O., Asare-Donkor, N. K., & Adimado, A. A. (2024). Binary Ce-doped-ZnO/rGO composite as excellent photocatalyst for bromothymol blue dye degradation. *Sustainable Chemistry for the Environment*, 5, 100069.
- Ullah, S., Shahid, W., Shahid, S., Khan, M. I., Ansar, N., Khizar, M., ... & Alreshidi, M. A. (2023). Advancing photocatalysis: Innovative approaches using novel $\text{V}_2\text{O}_5/\text{ZnO}$ nanocomposites for efficient photocatalytic degradation of tubantin red. *Journal of Saudi Chemical Society*, 27(6), 101766.
- Norouzi, A., & Nezamzadeh-Ejhih, A. (2020). Preparation, characterization, and investigation of the catalytic property of $\alpha\text{-Fe}_2\text{O}_3\text{-ZnO}$ nanoparticles in the photodegradation and mineralization of methylene blue. *Chemical Physics Letters*, 752, 137587.
- Norouzi, A., & Nezamzadeh-Ejhih, A. (2020). $\alpha\text{-Fe}_2\text{O}_3/\text{Cu}_2\text{O}$ heterostructure: Brief characterization and kinetic aspect of degradation of methylene blue. *Physica B: Condensed Matter*, 599, 412422.
- Aboutaleb, W. A., & El-Salamony, R. A. (2019). Effect of $\text{Fe}_2\text{O}_3\text{-CeO}_2$ nanocomposite synthesis method on the Congo red dye photodegradation under visible light irradiation. *Materials Chemistry and Physics*, 236, 121724.
- Arzaee, N. A., Betti, N., Al-Amiery, A., & Isahak, W. N. R. W. (2023). The role of tin species in doped iron (III) oxide for photocatalytic degradation of methyl orange dye under UV light. *Heliyon*, 9(7) e18076.
- Botsa, S. M., Naidu, G. P., Ravichandra, M., Rani, S. J., Anjaneyulu, R. B., & Ramana, C. V. (2020). Flower like $\text{SnO}_2\text{-}$

- Fe₃O₄-rGO ternary composite as highly efficient visible light induced photocatalyst for the degradation of organic pollutants from contaminated water. *Journal of Materials Research and Technology*, 9(6), 12461-12472.
9. Bameri, I., Saffari, J., Baniyaghoob, S., & Ekrami-Kakhki, M. S. (2022). Synthesis of magnetic nano-NiFe₂O₄ with the assistance of ultrasound and its application for photocatalytic degradation of Titan Yellow: Kinetic and isotherm studies. *Colloid and Interface Science Communications*, 48, 100610.
 10. Wang, R., Cao, J., Liu, J., & Zhang, Y. (2023). Synthesis of CuO@TiO₂ nanocomposite and its photocatalytic and electrochemical properties. Application for treatment of azo dyes in industrial wastewater. *International Journal of Electrochemical Science*, 18(12), 100316.
 11. Kabadayi, O., Altintig, E., & Ballai, G. (2024). Zeolite supported zinc oxide nanoparticles composite: Synthesis, characterization, and photocatalytic activity for methylene blue dye degradation. *Desalination and Water Treatment*, 100433.
 12. Saeed, M., Albalawi, K., Khan, I., Akram, N., Abd El-Rahim, I. H., Alhag, S. K., & Ahmed, A. E. (2023). Synthesis of pn NiO-ZnO heterojunction for photodegradation of crystal violet dye. *Alexandria Engineering Journal*, 65, 561-574.
 13. Ashiegbu, D. C., & Potgieter, H. J. (2023). ZnO-based heterojunction catalysts for the photocatalytic degradation of methyl orange dye. *Heliyon*, 9(10).
 14. Mohammed El Amine, Z., Tennouga, L., Brahim, B., & Belkaid, S. (2024). Removal of Methylene Blue Dye from an Aqueous Solution by an Adsorption Technique Using Sulfonated Polystyrene as Three Low-cost Adsorbents. *Physical Chemistry Research*, 12(2), 453-465.
 15. Foroutan, R., Peighambaridoust, S. J., Ghojavand, S., Foroughi, M., Ahmadi, A., Bahador, F., & Ramavandi, B. (2024). Development of a magnetic orange seed/Fe₃O₄ composite for the removal of methylene blue and crystal violet from aqueous media. *Biomass Conversion and Biorefinery*, 14(20), 25685-25700.
 16. Umesh, A. S., Puttaiahgowda, Y. M., & Thottathil, S. (2024). Enhanced adsorption: Reviewing the potential of reinforcing polymers and hydrogels with nanomaterials for methylene blue dye removal. *Surfaces and Interfaces*, 104670.
 17. Li, P., Zhang, J., Yu, Y., Jia, W., & Zhao, S. (2024). A collaborative coagulation strategy for algae-laden and dye-containing water treatment. *Journal of Cleaner Production*, 141146.
 18. Benalia, A., Derbal, K., Baatache, O., Lehchili, C., Khalfou, A., & Pizzi, A. (2024). Removal of Dyes from Water Using Aluminum-Based Water Treatment Sludge as a Low-Cost Coagulant: Use of Response Surface Methodology. *Water*, 16(10), 1400.
 19. Noor, M. H. M., & Ngadi, N. (2024). Global research landscape on coagulation-flocculation for wastewater treatment: A 2000–2023 bibliometric analysis. *Journal of Water Process Engineering*, 64, 105696.
 20. Pivokonsky, M., Novotna, K., Petricek, R., Cermakova, L., Prokopova, M., & Naceradska, J. (2024). Fundamental chemical aspects of coagulation in drinking water treatment—Back to basics. *Journal of Water Process Engineering*, 57, 104660.
 21. Ribeiro, J. P., Sarinho, L., & Nunes, M. I. (2024). Application of life cycle assessment to Fenton processes in wastewater treatment—A review. *Journal of Water Process Engineering*, 57, 104692.
 22. Yan, S., Liang, X., Liu, S., Zhang, Y., Zeng, J., Bai, J., ... & Li, J. (2024). Synthesis of PANI@ α-Fe₂O₃/Al₂O₃ photo-Fenton composite for the enhanced efficient methylene blue removal. *Journal of Sol-Gel Science and Technology*, 109(1), 137-149.
 23. Uluçtan, P. S., Eroğlu, H. A., Kadioğlu, E. N., & Akbal, F. (2025). Decolorization of Acid Red 337 dye with hydroxyl and sulfate radical based advanced oxidation processes using different iron Catalyst: An experimental and statistical Investigation. *Journal of Photochemistry and Photobiology A: Chemistry*, 459, 116105.
 24. Wu, T., Hu, Z., Yang, J., Jia, Y., Dong, Z., Tang, Y., & Zhang, Y. (2025). Insight into the roles of Cl⁻ for the degradation of Acid Red 14 in an electrochemical advanced oxidation system: Mechanisms and DFT studies. *Chemical Engineering Journal*, 503, 158079.
 25. Noshadi, E., Changizian, M., & Behbahani-Nejad, M. (2025). Enhancing wastewater treatment efficiency through hydrodynamic cavitation and advanced oxidation processes: Experimental insights and comparative analysis. *Journal of the Taiwan Institute of Chemical Engineers*, 166, 105604.
 26. Rini, N. P., Istiqomah, N. I., & Suharyadi, E. (2023). Enhancing photodegradation of methylene blue and reusability using CoO/ZnO composite nanoparticles. *Case Studies in Chemical and Environmental Engineering*, 7, 100301.
 27. Madkour, M., Allam, O. G., Abdel Nazeer, A., Amin, M. O., & Al-Hetlani, E. (2019). CeO₂-based nanoheterostructures with p-n and n-n heterojunction arrangements for enhancing the solar-driven photodegradation of rhodamine 6G dye. *Journal of Materials Science: Materials in Electronics*, 30, 10857-10866.
 28. El-Sayed, F., Ganesh, V., Hussien, M. S., AlAbdulaal, T. H., Zahran, H. Y., Yahia, I. S., ... & Bitla, Y. (2022). Facile synthesis of Y₂O₃/CuO nanocomposites for photodegradation of dyes/mixed dyes under UV-and visible light irradiation. *Journal of Materials Research and Technology*, 19, 4867-4880.
 29. Bukit, B. F., Pratama, A. W., Frida, E., Sedayu, B. B., Fransiska, D., Purnomo, D., ... & Syamani, F. A. (2025). Eco-friendly alginate/PCL-TiO₂ hybrid biocomposites: Preparation, properties, and methylene blue photodegradation. *South African Journal of Chemical Engineering*, 51, 254-264.
 30. Boucherdoud, A., Seghier, A., Kherroub, D. E., Douinat, O., Dahmani, K., Bestani, B., & Benderdouche, N. (2025). Autogenous deposition of copper oxide onto polyaniline nanocomposite catalysts for the photodegradation of methylene blue and congo red: Experimental inquiry, RSM optimization, and DFT calculation. *Materials Science and Engineering: B*, 314, 118015.
 31. Zhu, Y., Jiang, C., Meng, T., Yao, J., Peng, Z., Wang, P., ... & Zhao, Y. (2025). Heterojunction Engineering of g-C₃N₄ with Superior Photogenerated Electron Transfer for Boosting Photodegradation of Methylene Blue. *Optical Materials*, 116626.
 32. Hussain, M. H., & Pozan Soylu, G. S. (2025). Synthesis of Ionic Liquid-Assisted Nanoparticles: High Activity, Fast Removal for Photodegradation of Methylene Blue in Water. *Water, Air, & Soil Pollution*, 236(2), 1-20.
 33. Rini, N. P., Istiqomah, N. I., & Suharyadi, E. (2023). Enhancing photodegradation of methylene blue and reusability using CoO/ZnO composite nanoparticles. *Case Studies in Chemical and Environmental Engineering*, 7, 100301.
 34. Suliman, Z. A., Mecha, A. C., & Mwasiagi, J. I. (2024). Effect of TiO₂/Fe₂O₃ nanopowder synthesis method on visible light photocatalytic degradation of reactive blue dye. *Heliyon*, 10(8).
 35. Zeb, M., Anjum, Z., Mumtaz, S., Khalid, M., & Hafeez, M. (2024). Jasminum mesnyi mediated synthesis of Co₃O₄/NiO nanocomposite for methylene blue degradation. *Desalination and Water Treatment*, 317, 100165.
 36. Vallarasu, K., Dinesh, S., Mithun, D., Anitha, R., & Vijayalakshmi, V. (2024). ZnO heterojunction photocatalysts prepared via facile green synthesis process attaining improved photocatalytic function for degradation of methylene blue dye. *Desalination and Water Treatment*, 318, 100391.
 37. Kannan, K., Hemavathi, B., Radhika, D., Manjunath, H. R., Kumar, K., Lakkaboyana, S. K., ... & Raghu, A. V. (2024). Facile synthesis of novel ZnO-MgO nanohybrids and its photocatalytic degradation of toxic pollutants. *Desalination and Water Treatment*, 317, 100125.
 38. Alp, E., Eşgin, H., Kazmanlı, M. K., & Genc, A. (2019). Synergetic activity enhancement in 2D CuO-Fe₃O₄ nanocomposites for the photodegradation of rhodamine B. *Ceramics International*, 45(7), 9174-9178.
 39. Kim, S., Gupta, N. K., Bae, J., & Kim, K. S. (2021). Fabrication of coral-like Mn₂O₃/Fe₃O₄ nanocomposite for room temperature removal of hydrogen sulfide. *Journal of Environmental Chemical Engineering*, 9(3), 105216.
 40. Ghaffari, Y., Gupta, N. K., Bae, J., & Kim, K. S. (2020).

- One-step fabrication of Fe₂O₃/Mn₂O₃ nanocomposite for rapid photodegradation of organic dyes at neutral pH. *Journal of Molecular Liquids*, 315, 113691.
41. Baek, S., Ghaffari, Y., & Bae, J. (2022). Synthesis of Fe₂O₃/Mn₂O₃ nanocomposites and impregnated porous silicates for dye removal: insights into treatment mechanisms. *Catalysts*, 12(9), 1045.
 42. Yang, Z., Zhu, J., Tang, W., & Ding, Y. (2022). An Fe₂O₃/Mn₂O₃ Nanocomposite Derived from a Metal-Organic Framework as an Anode Material for Lithium-ion Batteries. *Chemistryselect*, 7(42), e202203107.
 43. Hassan, S. S., El-Shalakany, H. H., Fathy, M. A., & Kamel, A. H. (2024). A magnetic macroporous α -Fe₂O₃/Mn₂O₃ nanocomposite as an efficient adsorbent for simple and rapid removal of Pb (II) from wastewater and electronic waste leachate. *Environmental Science and Pollution Research*, 31(57), 65648-65660.
 44. Eslami, H., Ehrampoush, M. H., Esmaeili, A., Ebrahimi, A. A., Salmani, M. H., Ghaneian, M. T., & Falahzadeh, H. (2018). Efficient photocatalytic oxidation of arsenite from contaminated water by Fe₂O₃-Mn₂O₃ nanocomposite under UVA radiation and process optimization with experimental design. *Chemosphere*, 207, 303-312.
 45. Khalaji, A. D., & Jafari, E. (2023). Co-precipitation synthesis of α -Fe₂O₃: Characterization and their activities on photocatalytic degradation of methylene blue. *Inorganic Chemistry Research*, 7(1), 27-33.
 46. Khalaji, A. D., Palang Sangdevini, Z., Mousvi, S. M., Jarosova, M., & Macheh, P. (2021b). Benzoic acid-functionalized α -Fe₂O₃ nanoparticles: synthesis, characterization, magnetic and optical properties. *Asian J. Nanosci. Mater*, 4, 137-146.
 47. Sadeq, Z. S. (2019). Structural and optical study of Mn₂O₃ nanoparticles and its antibacterial activity. *Sylwan*, 161, 76-84.
 48. Sobhani, A. (2023). CuMn₂O₄/Mn₂O₃ micro composites: Sol-gel synthesis in the presence of sucrose and investigation of their photocatalytic properties. *Arabian Journal of Chemistry*, 16(10), 105201.
 49. Dhineshbabu, N. R., Rajendran, V., Nithyavathy, N., & Vetumperumal, R. (2016). Study of structural and optical properties of cupric oxide nanoparticles. *Applied Nanoscience*, 6, 933-939
 50. Boltaev, G. S., Ganeev, R. A., Krishnendu, P. S., Zhang, K., & Guo, C. (2019). Nonlinear optical characterization of copper oxide nanoellipsoids. *Scientific Reports*, 9(1), 11414.
 51. Deepthi, S., Vidya, Y. S., Manjunatha, H. C., Sridhar, K. N., Manjunatha, S., Munirathnam, R., & Ganesh, T. (2023). Comparison of cytotoxic and photoluminescence properties between Fe₂O₃ and Fe₃O₄. *Inorganic Chemistry Communications*, 156, 111101.
 52. Popa, A., Stefan, M., Macavei, S., Muresan, L. E., Leostean, C., Floare-Avram, C. V., & Toloman, D. (2023). Photoluminescence and Photocatalytic Properties of MWNTs Decorated with Fe-Doped ZnO Nanoparticles. *Materials*, 16(7), 2858.
 53. Shugabaev, T., Gridchin, V. O., Komarov, S. D., Kirilenko, D. A., Kryzhanovskaya, N. V., Kotlyar, K. P., ... & Cirilin, G. E. (2023). Photoluminescence redistribution of InGaN nanowires induced by plasmonic silver nanoparticles. *Nanomaterials*, 13(6), 1069.
 54. Kallawar, G. A., & Bhanvase, B. A. (2024). A review on existing and emerging approaches for textile wastewater treatments: challenges and future perspectives. *Environmental Science and Pollution Research*, 31(2), 1748-1789.
 55. Zafar, A. M., Naeem, A., Minhas, M. A., Hasan, M. J., Rafique, S., & Ikhlaq, A. (2024). Removal of reactive dyes from textile industrial effluent using electrocoagulation in different parametric conditions of aluminum electrodes. *Total Environment Advances*, 9, 200087.
 56. Weldegebrerial, G. K., & Sibhatu, A. K. (2021). Photocatalytic activity of biosynthesized α -Fe₂O₃ nanoparticles for the degradation of methylene blue and methyl orange dyes. *Optik*, 241, 167226.
 57. Salehzadeh, H., Wantala, K., Mohammadi, E., Shivaraju, H. P., Shahmoradi, B., Rtimi, S., ... & Safari, M. (2023). Solar photodegradation of malathion from aqueous media using Al-doped ZnO/Fe₃O₄ nanocomposite. *Catalysis Communications*, 184, 106785.
 58. Arumugaperumal, V., & Sadaiyandi, K. (2024). Solar light driven photocatalytic degradation of methylene blue dye over Cu doped α -MnO₂ nanoparticles. *Chemical Physics Impact*, 8, 100434.
 59. Basavanagoudra, H., Jangannanavar, V. D., Patil, M. K., Inamdar, S. R., & Goudar, K. M. (2024). Barium oxide nanorods: Catalyst concentration and surface defects' role in degrading methylene blue organic pollutant. *Chemical Physics Impact*, 8, 100578.
 60. Thambidurai, R., Gobi, G., Chandrasekar, M., Uthrakumar, R., Inmozhi, C., & Kaviyarasu, K. (2023). ZnO nanocomposites containing Cd are synthesized with high photodegradation potential for wastewater treatment. *Journal of King Saud University-Science*, 35(9), 102915.
 61. Widiyandari, H., Prilita, O., Al Ja'farawy, M. S., Nurosyid, E., Arutanti, O., Astuti, Y., & Mufti, N. (2023). Nitrogen-doped carbon quantum dots supported zinc oxide (ZnO/N-CQD) nanoflower photocatalyst for methylene blue photodegradation. *Results in Engineering*, 17, 100814.
 62. Liu, Y., Liu, T., Zhang, L., Wu, H., Guo, J., & Hu, X. (2023). One-pot synthesized NiFe₂O₄/CeO₂ composite catalyst for efficient degradation of methylene blue via photocatalysis under visible light. *Catalysis Communications*, 185, 106814.
 63. Makofane, A., Motaung, D. E., & Hintsho-Mbita, N. C. (2024). Green synthesis of silver deposited on copper ferrite nanoparticles for the photodegradation of dye and antibiotics. *Applied Surface Science Advances*, 21, 100601.
 64. Perumal, V., Uthrakumar, R., Chinnathambi, M., Inmozhi, C., Robert, R., Rajasaravanan, M. E., ... & Kaviyarasu, K. (2023). Electron-hole recombination effect of SnO₂-CuO nanocomposite for improving methylene blue photocatalytic activity in wastewater treatment under visible light. *Journal of King Saud University-Science*, 35(1), 102388.
 65. Weldekirstos, H. D., Mengist, T., Belachew, N., & Mekonnen, M. L. (2024). Enhanced photocatalytic degradation of methylene blue dye using facilely synthesized g-C₃N₄/CoFe₂O₄ composite under sun light irradiation. *Results in Chemistry*, 7, 101306.
 66. Chong, C. Y., Sum, J. Y., Lai, L. S., Toh, P. Y., & Chang, Z. H. (2024). Visible light-driven dye degradation by magnetic cobalt-doped zinc oxide/iron oxide photocatalyst. *Next Materials*, 2, 100074.
 67. Din, M. I., Khalid, R., Hussain, Z., Gul, S., & Mujahid, A. (2024). Synthesis and characterization of cobalt doped zinc oxide nanoparticles and their application for catalytic reduction of methylene blue dye. *Desalination and Water Treatment*, 317, 100002.
 68. Goudjil, M. B., Dali, H., Zighmi, S., Mahcene, Z., & Bencheikh, S. E. (2024). Photocatalytic degradation of methylene blue dye with biosynthesized Hematite α -Fe₂O₃ nanoparticles under UV-Irradiation. *Desalination and Water Treatment*, 317, 100079.
 69. Nguyen, T. T. D., Nguyen, D., Vo, P. P., Doan, H. N., Pham, H. T. N., Hoang, V. H., ... & Nguyen, P. T. (2023). The roles of ethanol and isopropanol as hole scavengers in the photoreduction reaction of graphene oxide by TiO₂: A competition of oxygenated groups removal and carbon defects invasion. *Journal of Molecular Liquids*, 381, 121831.
 70. Resende, J. E., Gonçalves, M. A., Oliveira, L. C., da Cunha, E. F., & Ramalho, T. C. (2014). Use of ethylenediaminetetraacetic acid as a scavenger for chromium from "wet blue" leather waste: Thermodynamic and kinetics parameters. *Journal of Chemistry*, 2014(1), 754526.
 71. Martín-Gómez, J., Pérez-Losada, M., López-Tenllado, F. J., Hidalgo-Carrillo, J., Herrera-Beurrio, M. C., Estévez, R., ... & Urbano, F. J. (2024). Insight into the reaction mechanism of photocatalytic production of solketal. *Catalysis Today*, 429, 114506.
 72. Henderson, M. A., & Shen, M. (2017). Electron-scavenging chemistry of benzoquinone on TiO₂ (110). *Topics in Catalysis*, 60, 440-445.